Extensively microtwinned diamond with nano-laminates of lonsdaleite formed by flash laser heating of glassy carbon

Brenton Cook[1], Philipp Reineck[1], Thomas Shiell[2], Jodie Bradby[2], Bryan D. Esser[3], Joanne Etheridge[3,4], Bianca Haberl[5], Reinhard Boehler[5], David R. McKenzie[6] and Dougal G. McCulloch[1*]

[1]Physics, School of Science, RMIT University, Melbourne, 3001, Australia.

[2]Research School of Physics, The Australian National University, Canberra, 2601, Australia.

[3]Monash Centre for Electron Microscopy, Monash University, Melbourne, 3800, Australia.

[4]School of Physics and Astronomy, Monash University, Melbourne, 3800, Australia.

[5]Neutron Scattering Division, Oak Ridge National Laboratory, Oak Ridge, Tennessee, 37830, USA.

[6]School of Physics, The University of Sydney, Sydney, 2006, Australia.

**Corresponding author dougal.mcculloch@rmit.edu.au*

Abstract

Diamond's unique properties on the nanoscale make it one of the most important materials for use in biosensors, quantum computing and for components that can withstand the harsh environments of space. We synthesise oriented, faceted diamond particles by flash laser heating of glassy carbon at 16 GPa and 2300 K. Detailed transmission electron microscopy shows them to consist of a mosaic of diamond nanocrystals frequently joined at twin boundaries forming microtwins. Striking three-fold translational periodicity was observed in both imaging and diffraction. This periodicity was shown to originate from nano-dimensional wedge-shaped overlapping regions of twinned diamond and not from a possible 9R polytype, which has also been reported in other group IVa elements and water ice. Extended bilayers of hexagonal layer stacking were observed, forming lonsdaleite nano-laminates. The particles exhibited optical fluorescence with a rapid quench time (<1 ns) attributed to their unique twinned microstructure.

Keywords: Diamond, defects, high pressure, laser heating, transmission electron microscopy

Defects in diamond are required to impart specialised functionality, for example the nitrogen vacancy centre, while others such as stacking faults and twinning have been shown to give high fracture toughness and unprecedented hardness[1,2]. These defects endow diamond with unique properties enabling applications in quantum communication and computing, biosensing and sensitive detection of ionising radiation in medical dosimetry[3,4]. However, defects may also lead to difficulties in the identification of the diamond polytypes present. For example, the presence of twins and stacking faults can lead to the incorrect identification of the hexagonal form of diamond known as lonsdaleite[5] and other proposed diamond polytypes[6]. Understanding the structure of defects at the nanoscale is needed to fully understand how they affect the properties of diamond. Annealing is frequently used to control the defect contents of crystals but its effects depend critically on the timing of the heating cycle. Laser heating creates conditions in which materials are raised for a brief time to high temperatures and quenched. This leads to the formation of phases that are the most energetically favourable that can be accessed in the limited time available. Novel materials are frequently produced because of the rapid temperature quenching which limits the formation of perfect crystals[7-10]. Under

pressure, pulsed or modulated laser heating of carbon has been found to produce a wide variety of crystalline and non-crystalline phases[11-14]. The rapid heating and cooling cycles also lead to materials that contain high levels of defects, which can influence properties. A key to unambiguously identifying defect structures at the atomic scale is high resolution electron microscopy.

Many solids including diamond consist of layers that can be stacked in various ways to give a structure with either cubic or hexagonal symmetry. Tetrahedrally bonded carbon can adopt an ABCABC… stacking sequence of its {111} layers leading to the cubic symmetry of diamond, or an ABAB… stacking sequence leading to the hexagonal symmetry of lonsdaleite[15]. The {111} layers also form the most common twin boundary in diamond, with the low energy $\Sigma 3$ <112>/<112> configuration being an example[16]. Variations in the stacking of the {111} layers leads to more complex polytypes of diamond which can have a combination of both cubic and hexagonal stacking sequences[11]. In addition to cubic diamond (3C) and hexagonal diamond (2H), other possible diamond polytypes have been proposed in theoretical studies including 4H, 6H, 8H, 10H, 9R, 12R, 15R and 21R[15,17]. An observation of one of these, 9R, has been claimed in diamond on the basis of three-fold translational periodicity in high resolution transmission electron microscope (TEM) images[18]. There have been reports of the 9R structure in chemical vapour deposited (CVD) diamond[19], Si[20,21] and SiC[22]. However, in the case of SiC, it was shown that a three-fold periodicity can possibly arise from certain types of twinning[23]. These questions are not limited to group IVa elements but also relevant to other systems that have both cubic and hexagonal stacking sequences as recently reported in water ice[24,25]. It remains an open question as to whether some of the apparent observations of 9R could be explained by the presence of twinning or other {111} stacking sequences.

In this work, we intentionally create diamond from compressed glassy carbon using modulated laser heating to a temperature close to the onset of diamond nucleation but below any melting (which yields large single crystal diamond upon recovery[13]). Glassy carbon was chosen as the precursor due to its isotropic, fully sp^2 bonded, sheet-like microstructure which has no preference for any one stacking sequence. High resolution electron microscopy is used to investigate the microstructure, including the nature of twinning present. In view of the importance of fluorescence in diamond, we also investigate the fluorescence behaviour of the resulting diamond.

Glassy carbon (Hochtemperatur-Werkstoffe Sigradur-G) was compressed in a diamond anvil cell with 440 µm diameter culets to a pressure of 16 GPa. A Re gasket with a pre-indented thickness of 50 µm was drilled with a 200 µm hole to act as the sample chamber in which the glassy carbon (~100 x 100 µm piece) was placed along with Ar as the pressure medium (Figure 1a). A ruby was also included to calibrate the pressure. The sample was irradiated using the method of laser flash-heating[26] employing an Yttrium Lithium Fluoride laser (YLF), at a wavelength of 1070 nm, with a single 40 ms square wave pulse. This method has previously been used for glassy carbon samples as detailed elsewhere[13]. The maximum temperature was measured to be 2350 ± 100 K using the grey body emission spectrum collected from the surface of the sample. This maximum temperature is constant during the entire flash with a heating time of ~1 ms and cooling time of ~1-2 ms[26]. The sample was recovered onto carbon-tape for *ex situ* analysis. A FEI SCIOS Dualbeam focused ion beam (FIB) was used prepare electron transparent lamellae from the irradiated region. The lamella was analysed using both conventional and aberration corrected transmission electron microscopy (TEM).

Figure 1b shows a cross-sectional TEM image of diamond particles formed near the surface of the sample after the flash laser heating process at 16 GPa. The temperature reached, but did not greatly exceed, the minimum temperature for diamond formation at this pressure and nucleated a few spatially separated diamond particles within the graphitic host. Our observation is in agreement with the temperature reported by Bundy et al. at 16 GPa for the rapid transformation of graphite to diamond (~2400K)[27]. Some of the larger diamond particles protrude from the surface, suggesting a growth process whereby nucleation occurs just below the surface. Other diamond crystals grow entirely within the glassy carbon host showing decreasing size and frequency with increasing depth below the surface, consistent with a decreasing maximum temperature. The SEM image in the inset of Figure 1b shows the protruding particles and their distinctive faceted morphology, including occasional trigonal and pentagonal shapes. These morphologies have been observed in diamond formed using CVD which contain twins[28]. Elemental analysis of the diamond particles using energy dispersive spectroscopy (EDS) found no evidence of impurities.

Figure 1c shows a TEM image of a one of the larger diamond crystals formed at the surface. A typical selected area diffraction pattern collected from this particle is shown in Figure 1d. In addition to the strong reflections which are indexed to cubic diamond oriented along <110>, secondary diffraction spots (indicated by arrows) are evident with a periodicity three times that of the diamond {111} d-spacing. These secondary spots are present in both <111> directions visible, consistent with the presence of two district orientations of the structure in equal amounts with an angle of 120° between them. The presence of three-fold periodicity has been previously used as evidence for the 9R polytype of diamond[18,19] and in other materials with the diamond cubic structure[20-22]. Figure 1e shows a schematic of the stacking sequence of the {111} layers in the 9R structure compared to diamond. Calculated diffraction patterns for an equal mix of 9R diamond crystals with their c-axes at an angle of 120° are compared to the experiment in Figure 1f (as blue and red spots overlayed on the diffraction pattern). While the 9R structure gives a good match to some of the observed diffraction spots along the major axes of the pattern, many other predicted spots of 9R are not consistent with experiment (see for example arrows in Figure 1f). The observed pattern was also not consistent with any other rotation of the 9R crystal, ruling out the possibility that this phase is the cause of the three-fold periodicity.

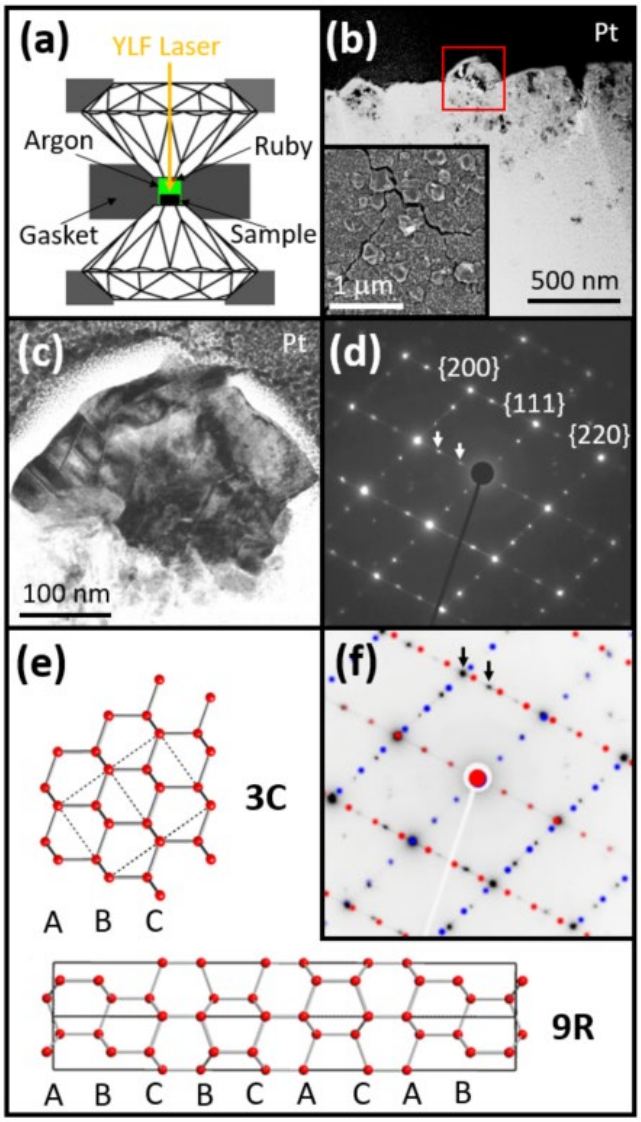

Figure 1. (a) Schematic of the diamond anvil cell used to produce the flash laser heated glassy carbon samples, which were loaded in an Ar pressure medium, compressed to 16 GPa and heated to 2350 K using an Yttrium Lithium Fluoride laser (YLF). (b) Cross-sectional TEM image of the surface region of the GC after the flash laser heating. The inset shows a scanning electron microscope image of the faceted diamond particles formed below and protruding from the surface. (c) TEM image of one of the larger diamond particles protruding from the surface (indicated by the red box in (b)). (d) Diffraction pattern from the particle in (c) with the main reflections indexed to diamond, looking along <110>. Additional diffraction spots are evident with a periodicity 3 times that of the diamond {111} d-spacing along both <111> directions (indicated by arrows). (e) The 9R structure consisting of ABCBCACAB stacking of {111} layers compared to regular ABC stacking in diamond cubic (3C). (f) Calculated diffraction patterns (red and blue) of two overlapping 9R crystals at an angle of 120°, each with their c-axis along a <111> direction of diamond, overlayed on the experiment.

Many observed reflections are not correctly predicted (some indicated by arrows) showing that this proposed 9R model is not correct.

A high resolution TEM image (FEI Double-corrected Titan FEGTEM) of a region of crystal exhibiting the three-fold periodicity is shown in Figure 2a. The image shows regions of defect-free diamond (see Fourier transform (FFT) in Figure 2b) and regions with extensive microtwinning and grain boundaries. A FFT of a typical region with three-fold periodicity is shown in Figure 2c, revealing the periodicity occurs in one, and only one, of the <111> directions. The pattern of spots in the FFT is rectangular (indicated by the dashed rectangle) which has previously been observed in cubic SiC and shown to be inconsistent with the 9R structure which would produce a parallelogram[23]. Note that previous reports of the 9R structure in both diamond[18,19] and silicon[21] have this same rectangular pattern in the FFT of their images, casting doubt on the claims of the presence of 9R in those cases.

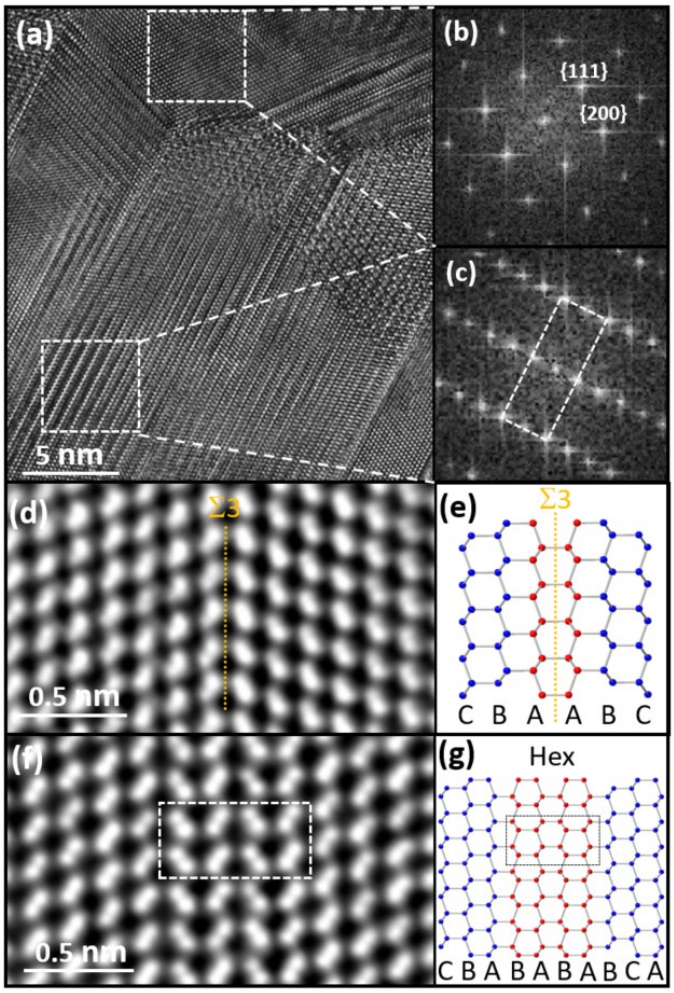

Figure 2 (a) High resolution bright field TEM image of a typical region of extensively microtwinned diamond along <111> directions with a mosaic of related structures. (b) A FFT of a region of defect-free diamond (indicated in (a)). (c) A typical FFT of one the regions in (a) with 3-fold periodicity of three {111} layers along one of the <111> directions of diamond. The white box indicates the orthogonal alignment of the spots which is not consistent with the 9R structure. (d) The most common type of twin with the low energy Σ3 <112>/<112> configuration at a {111} twin boundary (shown by the model in (e)) imaged using iDPC-STEM. (f) An example of a hexagonal ABAB sequence (highlighted by the dashed rectangles) consisting of two sets of {111} layers surrounded by ABC cubic diamond (as shown in the model (g)) imaged using iDPC-STEM.

Figure 2d shows a high-resolution iDPC-STEM image[29] (Thermo Scientific Spectra ϕ FEGTEM) of the most common type of twin observed in the sample, which can be categorised as a low energy Σ3 <112>/<112> configuration at a {111} twin boundary (as shown in the structural model of Figure 2e). In addition to twinning, the same sample contained other {111} stacking sequences. Figure 2f shows, for example, a change from a cubic ABC sequence to a hexagonal ABAB sequence and then back to cubic again. The presence of changes of cubic to hexagonal stacking has been

observed previously in diamond formed near the graphite/diamond phase boundary[11]. Such mixed stacking of {111} diamond layers is a likely result of the rapid quench that took place in our sample that limited the time for the layers to find the most energetically favoured (cubic) sequence.

Figure 3a shows an enlargement of a region of Figure 2a in which the <110> diamond lattice image progressively changes (from left to right) into an image that exhibits the characteristic three-fold periodicity. This type of progressive change in the image has been observed in cubic SiC[22,23] when viewed along <110> and was attributed to overlapped crystals joined at a twin boundary. Each crystal when viewed along <110> has the form of a wedge as shown in Figure 3b with either a {111}/{115} or a {112}/{112} twin boundary[23]. A simulated image (created using *muSTEM*[30]) of this configuration is shown in Figure 3c exhibiting the same progressive change from diamond to the three-fold periodic pattern, consistent with our experimental images. Also shown in Figure 2d is a model looking down <110> of diamond which is partially overlapped with the second crystal in which the three-fold periodicity is apparent in the overlapped section. We therefore conclude that our sample has a high content of twinning at the microscopic scale, in all <111> directions.

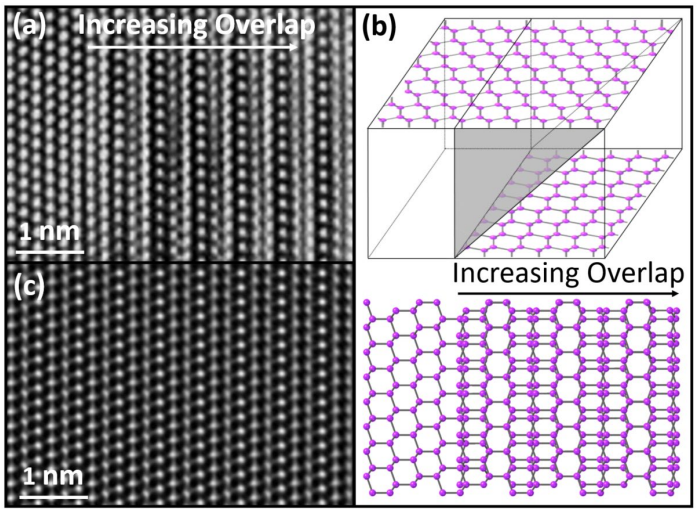

Figure 3 (a) TEM image showing the threefold translational periodicity developing with increasing overlap (in the direction indicated) of diamonds meeting at a twin boundary. (b) Schematic of two overlapping <110> diamond crystals in the form of wedges. (c) A calculated image using the geometry shown in (b) in which the degree of overlap increases from left to right as in (a). (d) The projection of overlapped regions of model exhibiting the same type of three-fold translational periodicity seen in the images.

It is of interest to characterize the effect of the type of microtwinning observed in our sample on the fluorescence behaviour. Fluorescence is used in assessing the monetary value of gem quality diamond and is important in developing new applications of diamond for optical devices. The confocal fluorescence image of the surface of the sample is shown in Figure 4a, with the protruding diamond particles fluorescing strongly when illuminated with 520 nm light. The normalised fluorescence spectrum from our sample (red trace in Figure 4b) shows some of the typical spectral characteristics of fluorescence from the nitrogen-vacancy (NV) defect (also referred to as the NV centre), which is one of the most common and the most studied fluorescent defects in diamond. A typical fluorescence spectrum of nanodiamond containing ~3 ppm of NV centres is shown for comparison (black trace). None of the locations investigated in our sample exhibited the so-called NV^0 and NV^- zero-phonon lines at 575 nm and 637 nm, respectively, which are characteristic narrow peaks typically seen in NV fluorescence spectra. However it is known that these are not necessarily present in diamond nanoparticles[31]. The peak at ~558 nm is where the diamond Raman peak (1332 cm^{-1}) is expected for the 520 nm excitation used here, albeit much broader than in bulk diamond. The spectral width of the diamond Raman line is partially caused by the spectrally broad excitation beam used here (520 ± 10 nm). It is also known that the Raman line of nanocrystals can be significantly broader than that observed for bulk diamond[32].

Interestingly, the fluorescence decay time of our sample (< 1ns) is significantly shorter than that observed from the nanodiamonds (~ 19 ns). Typical NV centre decay times in diamond nanoparticles exceed 20 ns[31] but it is known that

the presence of nearby defects can shorten the fluorescence lifetime of NV centers[33,34]. Therefore it is likely that the presence of microtwinning has dramatically shortened the NV lifetime. The inset in Figure 4c shows normalised fluorescence spectra of microtwinned diamond particles for excitation wavelengths of 520 nm, 500 nm and 470 nm. The fluorescence peak position slightly blue-shifts with decreasing excitation wavelength, accompanied by a pronounced increase in fluorescence intensity around 600 nm. Both observations are consistent with a more efficient excitation of NV^0 relative to NV^- at shorter excitation wavelengths[35]. The emission peak at 558 nm for 520 nm excitation disappears for shorter excitation wavelengths, further supporting that it is a Raman signal and not fluorescence. A material such as microtwinned diamond that combines exceptional thermal and mechanical properties[1,2] with fast optical response times is both rare and highly desirable, especially for emerging applications in the extreme environments of space.

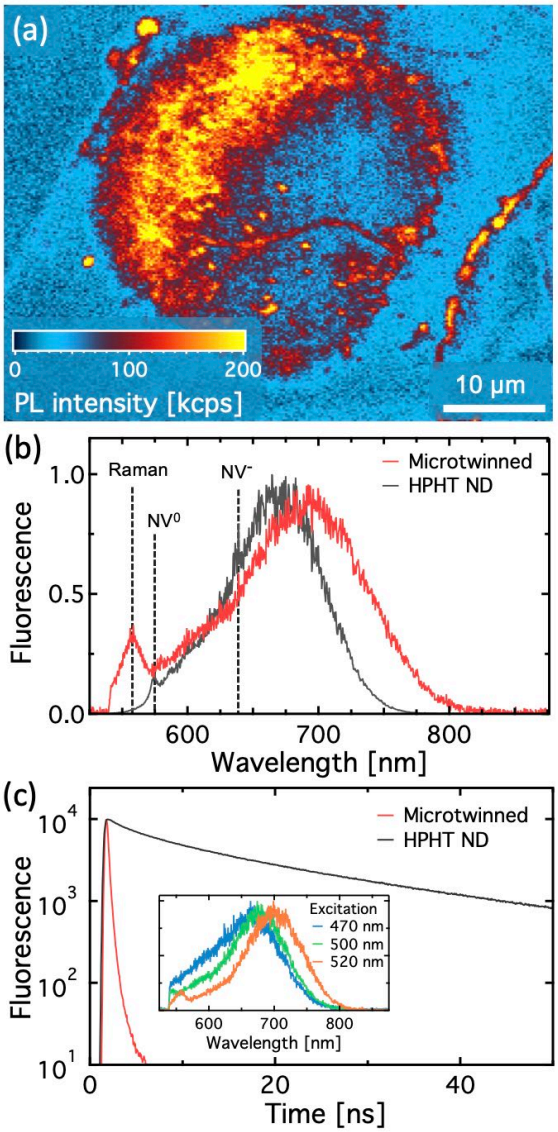

Figure 4. (a) Confocal photoluminescent (PL) imaging of the surface of the sample after recovery from the DAC acquired using 520 nm light excitation light. (b) Spectrum of the fluorescent light collected from our microtwinned diamond compared to nanodiamond (ND) prepared using high pressure and high temperature (HPHT) synthesis. (c) The corresponding time-resolved fluorescence decay traces for the samples in (b) acquired using a picosecond pulsed laser.

In summary, rapid temperature transients that briefly cause glassy carbon to enter the diamond nucleation region of the phase diagram of carbon forms diamond particles with extensive microtwinning at {111} planes. This type of microstructure can lead to distinctive three-fold periodicity in TEM images, which we show is not due to the presence of the 9R polytype of diamond but rather overlapping crystal wedges joined at {111} twin boundaries. This result shows that TEM images from structures that have both cubic and hexagonal stacking sequences should be carefully interpreted to avoid confusion between twinning and new polytypes. Variations of {111} stacking sequences were also observed in our sample including a brief transition into the hexagonal (lonsdaleite) sequence. Consequence of the

extensively microtwinned microstructure found in our sample are a 20 times shorter decay time of the fluorescence of the NV centre in diamond. This short quench time has potential to refine the properties of diamond for use in biosensors and optically mediated applications.

Acknowledgments

Electron microscopy was conducted at the RMIT Microscopy and Microanalysis Facility and the Monash Centre for Electron Microscopy. The authors gratefully acknowledge support for this research provided by Australian Research Council. This research used resources at the Spallation Neutron Source, a DOE Office of Science User Facility operated by the Oak Ridge National Laboratory.

References

(1) Huang, Q.; Yu, D.; Xu, B.; Hu, W.; Ma, Y.; Wang, Y.; Zhao, Z.; Wen, B.; He, J.; Liu, Z.; Tian, Y. Nanotwinned diamond with unprecedented hardness and stability, *Nature*, **2014**, 510, 250-253.
(2) Yue, Y.; Gao, Y.; Hu, W.; Xu, B.;Wang, J.; Zhang, X.; Zhang, Q.; Wang, Y.; Ge, G.; Yang, Z.; Li, Z., Ying, P.; Liu, X.; Yu, D., Wei, B.; Wang, Z.; Zhou, X-F.; Guo, L.; Tian, Y. Hierarchically structured diamond composite with exceptional toughness**,** *Nature*, **2020**, 582, 370-374.
(3) Ruf, M., Wan, N.H., Choi, H., Englund, D., Hanson, R. Quantum networks based on color centers in diamond, *J. Appl. Phys.*, **2021**, 130, 070901.
(4) Aslam, N., Zhou, H., Urbach, E.K., Turner, M.J., Walsworth, R.L, Lukin, M.D. Quantum sensors for biomedical applications. *Nat. Rev. Phys.,* **2023**, 5, 157.
(5) Németh, P.; Garvie, L.A.J.; Aoki, T.; Dubrovinskaia, N.; Dubrovinsky, L.; Buseck, P.R. Lonsdaleite is faulted and twinned cubic diamond and does not exist as a discrete material, *Nat. Commun.*, **2014**, 5, 5447.
(6) Németh, P.; Garvie, L.A.J.; Buseck, P.R. Twinning of cubic diamond explains reported nanodiamond polymorphs, *Sci. Rep.*, **2015**, 5, 18381.
(7) Horstmann, J.G.; Wit, W., Storeck, G.; Ropers, C. Coherent control of a structural phase transition in a solid-state surface system, *Nature*, **2020**, 583, 232.
(8) Nova, T.F.; Disa, A.D.; Fechner, M.; Cavalleri, A. Metastable ferroelectricity in optically strained SrTiO3, *Science*, **2019**, 364, 1075.
(9) Rapp, L.; Haberl, B.; Pickard, C.J.; Bradby; J.E., Gamaly; E.G. Williams; J.S.; Rode, A.V. Experimental evidence of new tetragonal polymorphs of silicon formed through ultrafast laser-induced confined microexplosion", *Nature Mater.* **2015**, 6, 7555.
(10) Rode, A.V.; Hyde, S.T.; Gamaly, E.G.; Elliman, R.G.; McKenzie, D.R., Bulcock, S. Structural analysis of a carbon foam formed by high pulse-rate laser ablation, *Appl. Phys. A*, **1999**, 69, S755.
(11) Yusa, H. Nanocrystalline diamond directly transformed from carbon nanotubes under high pressure. *Diam. Relat. Mater.* **2002**, 11, 87.
(12) Joshi, P.; Riley, P.; Gupta, S.; Narayan, R.J.; Narayan J. Advances in Laser-Assisted Conversion of Polymeric and Graphitic carbon into Nanodiamond Films. *Nanotechnology*. **2021**, 32, 432001.
(13) Yang, L.; Karandikar, A.; Shiell,T.B.; Cook, B. A.; Wong, S.; Field, M.R.; Bradby, J.E.; Haberl, B.; McCulloch, D.G.; Boehler, R. Melting diamond in the diamond cell by laser-flash heating, *High Pressure Research*, **2023**, 43, 1.
(14) Bhaumik, A.; Narayan, J. Nano-to-micro diamond formation by nanosecond pulsed laser annealing, *J. Appl. Phys.* **2019**, 126, 125307.
(15) Phelps, A.W.; Howard, W.; Smith, D.K. Space groups of the diamond polytypes, *J. Mater. Res.,* **1993**, 8, 2835.
(16) Zhang, Y.; Ichinose, H.; Nakanose, M.; Ito K.; Ishida, Y. Structure modelling of $\Sigma 3$ and $\Sigma 9$ coincident boundaries in CVD diamond thin films. *J. electron microsc.*, **1999**, 48, 246.
(17) Wen, B.; Zhao, J.; Bucknum, M.J.; Yao, P.; Li, T. First-principles studies of diamond polytypes. *Diam. Relat. Mater.* **2008**, 17, 356–364.
(18) Lifshitz, Y.; Duan, X.F.; Shang, N.G.; Li, Q.; Wan, L.; Bello, I.; Lee, S.T. Epitaxial diamond polytypes on silicon. *Nature,* **2001**, 412, 404.
(19) Zhu, W.; Badzian, A. R.; Messier, R.; Structural imperfections in CVD diamond films. *J. Mater. Res.* **1989**, 4, 659–663.

(20) Liu, X.; Wang, D. Kinetically-induced hexagonality in chemically grown silicon nanowires. *Nano Res.* **2009**, 2, 575–582.
(21) Smillie, L.A.; Niihori, M.; Rapp, L.; Haberl, B.; Williams, J.S.; Bradby, J.E.; Pickard, C.J.; Rode, A.V. Exotic silicon phases synthesized through ultrashort laser-induced microexplosion: Characterization with Raman microspectroscopy. *Phys. Rev. Mater.*, **2020**, 4, 093803.
(22) Jepps, N.W.; Page, T.F. 9R-HREM Observations of a New Silicon Carbide Polytype. *J. Am. Ceram. Soc.* **1980**, 63, 102-103.
(23) Kaiser, U.; Chuvilin, A.; Brown, P.D.; Richter, W. Origin of Threefold Periodicity in High-Resolution Transmission Electron Microscopy Images of Thin Film Cubic SiC. *Microsc. Microanal.* **1999**, 5, 420–427.
(24) Salzmann, C.G.; Murray, B.J. Ice goes fully cubic. *Nature Mater*. **2020**, 19, 586-587
(25) Huang, X.; Wang, L.; Liu, K.; Liao, L.; Sun, H.; Wang, J.; Tian, X.; Xu, Z.; Wang, W.; Liu, L.; Jiang, Y.; Chen, J.; Wang E.; Bai, X. Tracking cubic ice at molecular resolution, *Nature*. **2023**, 617, 86-91.
(26) Yang L, Karandikar A, Boehler R. Flash heating in the diamond cell: Melting curve of rhenium. *Rev Sci Instrum.* **2012**, 83, 063905.
(27) Bundy, F.P.; Bassett, W.A.; Weathers, M.S.; Hemley, R.J.; Mao, H.U.; Goncharov, A.F. The pressure-temperature phase and transformation diagram for carbon; updated through 1994, *Carbon*. **1996**, 34, 141–153.
(28) Wang, Z.L.; Bentley, J.; Clausing R.E.; Heatherly, L.; Horton, L.L. Direct correlation of microtwin distribution with growth face morphology of CVD diamond films by a novel TEM technique, *J. Mater. Res.*, **1994**, 9, 1552-1565.
(29) Lazic, I.; Bosch, E.G.T.; Lazar, S. Phase contrast STEM for thin samples: Integrated differential phase contrast, *Ultramicroscopy*. **2016**, 160, 265-280.
(30) Allen, L.J.; D'Alfonso, A.J.; Findlay, S.D. Modelling the inelastic scattering of fast electrons, *Ultramicroscopy*. **2015**, 151, 11-22.
(31) Reineck, P.; Trindade, L.F.; Havlik, J.; Stursa, J.; Heffernan, A.; Elbourne, A.; Orth, A. Capelli, M.; Cigler, P.; Simpson, D.A.; Gibson, B.C. Not All Fluorescent Nanodiamonds Are Created Equal: A Comparative Study. *Part. Part. Syst. Charact.* **2019**, 36, 1900009.
(32) Mermoux, M.; Chang, S.; Girard, H.A.; Arnault, J-C. Raman spectroscopy study of detonation nanodiamond. *Diam. Relat. Mater.* **2018**, 87, 248–260.
(33) Capelli, M.; Lindner, L.; Luo, T.; Jeske, J.; Abe, H.; Onoda, S.; Ohshima, T.; Johnson, B.; Simpson, D.A.; Stacey, A. Proximal nitrogen reduces the fluorescence quantum yield of nitrogen-vacancy centres in diamond. *New J. Phys.* **2022**, 24, 033053.
(34) Mizuno, K.; Nakajima, M.; Ishiwata, H.; Hatano, M.; Iwasaki, T. Electron spin contrast of high-density and perfectly aligned nitrogen-vacancy centers synthesized by chemical vapor deposition. *Appl. Phys. Express.* **2021**, 14, 032001.
(35) Aslam, N.; Waldherr, G.; Neumann, P.; Jelezko, F.; Wrachtrup, J. Photo-induced ionization dynamics of the nitrogen vacancy defect in diamond investigated by single-shot charge state detection, *New J. Phys.* **2013**, 15, 013064.

TOC graphic